THE JOURNAL OF PHYSICAL CHEMISTRY B

Article

pubs.acs.org/JPCB

SRLS Analysis of ^{15}N Relaxation from Bacteriophage T4 Lysozyme: a Tensorial Perspective That Features Domain Motion

Eva Meirovitch*

The Mina and Everard Goodman Faculty of Life Sciences, Bar-Ilan University, Ramat-Gan 52900 Israel

ABSTRACT: Bacteriophage T4L lysozyme (T4L) comprises two domains connected by a helical linker. Several methods detected *ns* domain motion associated with the binding of the peptidoglycan substrate. An ESR study of nitroxide-labeled T4L, based on the slowly relaxing local structure (SRLS) approach, detected *ns* local motion involving the nitroxide and the helix housing it. ^{15}N−H spin relaxation data from T4L acquired at magnetic fields of 11.7 and 18.8 T, and 298 K, were analyzed previously with the model-free (MF) method. The results did not detect domain motion. SRLS is the generalization of MF. Here, we apply it to the same data analyzed previously with MF. The restricted local N−H motion is described in terms of tilted axial local ordering ($\boldsymbol{S}$) and local diffusion ($\boldsymbol{D}_2$) tensors; dynamical coupling to the global tumbling is accounted for. We find that $D_{2,\perp}$ is 1.62×10^7 (1.56×10^7) s^{-1} for the N-terminal (C-terminal) domain. This dynamic mode represents domain motion. For the linker $D_{2,\perp}$ is the same as the rate of global tumbling, given by $(1.46 \pm 0.04) \times 10^7 s^{-1}$. $D_{2,\|}$ is 1.3×10^9, 1.8×10^9 and 5.3×10^9 s^{-1} for the N-terminal domain, the C-terminal domain, and the linker, respectively. This dynamic mode represents N−H bond vector fluctuations. The principal axis of $\boldsymbol{D}_2$ is virtually parallel to the N−H bond. The order parameter, S_0^2, is 0.910 ± 0.046 for most N−H bonds. The principal axis of $\boldsymbol{S}$ is tilted from the C_{i-1}^{α}−C_i^{α} axis by −2° to 6° for the N-, and C-terminal domains, and by 2.5° for the linker. The tensorial-perspective-based and mode-coupling-based SRLS picture provides new insights into the structural dynamics of bacteriophage T4 lysozyme.

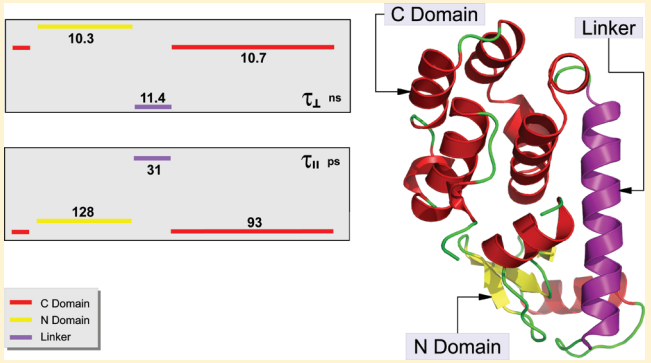

1. INTRODUCTION

Bacteriophage T4 lysozyme (T4L) is an endoacetyl-muramidase produced late in the infection of *Escherichia coli* by T4 bacteriophage.[1,2] The T4L molecule (Figure 1)[3] comprises an N-terminal domain (residues 13−65), a C-terminal domain (residues 1−10 and 81−164), and an intervening helical linker (residues 66−80). The sugar moiety of the peptidoglycan substrate binds in the cleft formed between the two domains. A large number of experimental and theoretical studies have been carried out on wild-type (WT) T4L, T4L mutants and T4L complexes.[3−24]

The theoretical methods used include the coarse-grained Gaussian network model,[6] essential dynamics (ED),[8] a method called amplified collective motions,[10] and conventional molecular dynamics (MD).[7−10] The ED-based study provides extensive details associated with the nature of domain mobility. Collective fluctuations have been derived from 1 ns long MD trajectories, and from a distribution of 21 PDB crystal structures of the WT protein and various mutants.[8] In both cases, the collective fluctuations have been shown to describe domain motion. A domain-closure mode, and a twisting mode, both associated with substrate-binding, represent the dominant large-amplitude dynamic processes. Localized bond-vector fluctuations have also been reported.[8]

An early X-ray crystallography study, which determined the 3LZM structure, detected apparent motion in the crystal. This

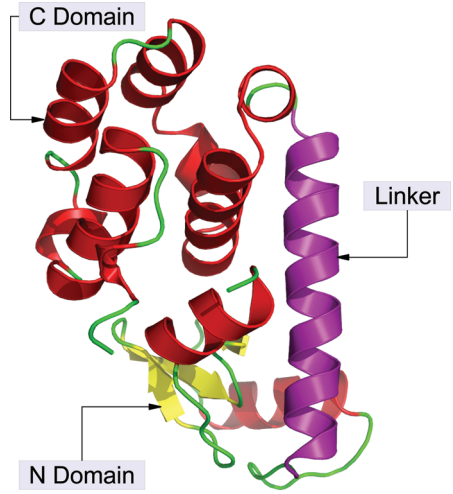

Figure 1. Ribbon diagram of the backbone of T4L based on the crystal structure 3LZM, with the N-terminal domain, the C-terminal domain and the linker demarcated (following the presentation of ref 3).

Received: February 29, 2012
Revised: April 17, 2012
Published: May 8, 2012

process could be interpreted in terms of opening and closing of the active site cleft.[4] The N-terminal domain engages in this important motion inherently; the C-terminal domain does so mainly by virtue of crystal contacts.[5] Information on hierarchial folding, with certain elements of the C-terminal domain acting as nucleation sites, was also reported.[12]

A residual dipolar coupling study determined the relative orientations of the T4L domains in solution.[11] An average structure that is more open than the 3LZM crystal structure was found to prevail in the liquid state. This is an important finding, rationalizing the entry of the relatively large substrate into the interdomain binding site cleft. The average solution structure is brought about by fast (on the chemical shift time scale) exchange among the members of a conformational ensemble that most likely extends from very open conformations to the maximally closed conformation. Although direct information on the rate of this process was not obtained, the results are consistent with *ns* conformational exchange interpretable as domain motion.

T4L was studied extensively with ESR of nitroxide-labeled T4L. A total of 36 different samples, with the nitroxide radical attached to the protein at different positions, have been prepared and investigated.[3,13−16] The relative importance of tertiary structure interactions, the chemical nature of the tether, and backbone fluctuations in establishing protein dynamics was assessed. It was suggested that the backbone fluctuations detected occur on the *ns* time scale.

Relatively simple dynamic models were used in the earlier ESR studies.[3,13−16] Subsequently, methods of data analysis based on the stochastic Liouville equation were applied.[17,18] Recently, the two-body coupled-rotator slowly relaxing local structure (SRLS) model of Freed and co-workers[19−21] was used to study the structural dynamics of nitroxide-labeled T4L.[22−24] The multifrequency temperature-dependent data sets employed in ref 24 has provided a comprehensive physical picture of the different motional modes experienced by the nitroxide. The rates of these dynamic modes have been determined, and a detailed description of the local ordering prevailing at the site where these motions take place has been elucidated. Among others, a motional mode on the order of *ns* involving the nitroxide, and the α-helix housing it, was detected.[23,24]

NMR spin relaxation is a powerful method for studying protein dynamics.[25−27] The ^{15}N−^{1}H bond is a particularly useful probe. The authors of ref 11 acquired ^{15}N−H T_1, T_2 and ^{15}N−{^{1}H} *NOE* from T4L at magnetic fields of 11.7 and 18.8 T, and 298 K, and subjected these data to model-free (MF)[28−30] analysis. The results did not bear out domain motion. A likely reason is the simple nature of MF. If the N- and C-terminal domains indeed reorient internally on the nanosecond time scale, where the global tumbling occurs, dynamical coupling between the internal and global motions cannot be ignored. Yet, mode-coupling is outside the scope of MF. We[31−42] and others[43−48] found previously that the asymmetry of the local spatial restrictions at N−H sites in proteins is an important factor. To account for it in spin relaxation analysis, a general tensorial representation of the local ordering and the local motion is required.[31−34,41] Yet, MF only accounts for the simplest tensor symmetry and local geometry.

SRLS is the generalization of MF. It treats the local ordering and the local diffusion as rank 2 tensors, and it accounts for mode-coupling. In this study, we apply SRLS, as developed for NMR spin relaxation in proteins,[31−34,41] to the same data analyzed previously[11] with MF. On the basis of the insightful results obtained by applying SRLS/ESR to nitroxide-labeled T4L,[23,24] we expect to obtain insightful information, in particular on internal domain mobility, by applying SRLS/NMR to ^{15}N−H relaxation from T4L.

SRLS/NMR was applied in the past to ^{15}N−H relaxation from *E. coli* adenylate kinase (AKeco),[35,36] which also experiences *ns* domain motion undetected by MF.[33] In that case, we accounted for the asymmetry of the local spatial restrictions, which must be addressed, by allowing for rhombic local potentials/local ordering tensors.[33,34,39,41] This is appropriate but computationally demanding for the structurally preserved parts of the polypeptide chain. For practical reasons, only the internally mobile domains of AKeco were analyzed in detail. In this study, we use a different scheme for representing the asymmetry of the local spatial restrictions: we allow for properly tilted axial local ordering ($\boldsymbol{S}$) and local diffusion ($\boldsymbol{D}_2$) tensors.[40,42] This representation is less straightforward but appropriate,[40,42] while the calculations are substantially more effective.

As shown below, the SRLS analysis of the ^{15}N−H relaxation data from T4L indeed provided a new picture of structural dynamics that features *ns* domain motion. The dynamic mode representing this process is given by $D_{2,\perp}$, the perpendicular component of the local diffusion tensor. Domain motion occurs in the presence of strong local ordering described by a tensor with principal value of approximately 0.9, and principal axis nearly parallel to the C^{α}_{i-1}−C^{α}_{i} axis. Fast N−H bond vector fluctuations around the equilibrium N−H orientation, occurring with correlation times of 30−125 ps, are given by $D_{2,\parallel}$, the parallel component of the local diffusion tensor.

Mode-coupling is obviously important when the internal motion of large domains is comparable in rate to the global tumbling.[33,41] That elucidation of insightful structural dynamics in proteins, in general, and the detection of domain motion in T4L, in particular, are contingent on a tensorial perspective in treating ^{15}N spin relaxation in proteins, is perhaps less obvious. The present SRLS-based analysis promotes the tensorial perspective in the context of mode-coupling. It may be considered a paradigm for physically sound and computationally effective analysis of NMR spin relaxation from flexible multidomain proteins/enzymes.

A theoretical background is provided in section 2. Results and Discussion constitute section 3. Our conclusions appear in section 4.

2. THEORETICAL BACKGROUND

2.1. The Slowly Relaxing Local Structure Approach. The two-body coupled-rotator SRLS theory[19−21] as applied to NMR spin relaxation in proteins is outlined in refs 31−34. A brief summary is given below. The SRLS frames are shown in Figure 2A. LF is the space-fixed laboratory frame with its *Z*-axis parallel to the external magnetic field. M1F is the principal axis system (PAS) of the global diffusion tensor, $\boldsymbol{D}_1$. VF is the local director given in this case by the average N−H orientation. The M1F and VF frames are fixed in the protein. The OF frame is the PAS of the local ordering tensor, $\boldsymbol{S}$; the M2F frame is the PAS of the local diffusion tensor, $\boldsymbol{D}_2$. DF is the PAS of the magnetic ^{15}N−^{1}H dipolar tensor, and CF is the PAS of the ^{15}N chemical shift anisotropy (CSA) tensor. OF, M2F, DF, and CF are fixed in the probe.

Figure 2B shows the various frames in the context of the protein (blue ellipse) and the probe (red ellipse). The time

dx.doi.org/10.1021/jp301999n | J. Phys. Chem. B 2012, 116, 6118−6127

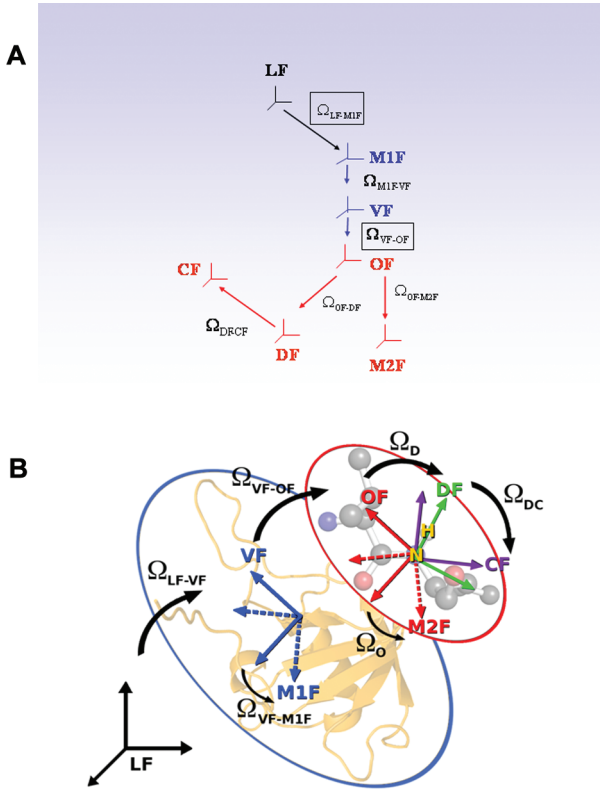

Figure 2. (A) LF is the space-fixed laboratory frame with its Z-axis parallel to the external magnetic field. M1F is the principal axis system (PAS) of the global diffusion tensor, $\boldsymbol{D}_1$. VF is the local director. The M1F and VF frames are fixed in the protein (blue). The OF frame is the PAS of the local ordering tensor, $\boldsymbol{S}$. M2F is the PAS of the local diffusion tensor, $\boldsymbol{D}_2$. DF is the PAS of the magnetic $^{15}N-^{1}H$ dipolar tensor. CF is the PAS of the ^{15}N chemical shift anisotropy tensor. OF, M2F, DF, and CF are fixed in the probe (red). The Euler angles Ω_{M1F-VF}, Ω_{OF-M2F}, Ω_{OF-DF}, and Ω_{DF-CF} are time-independent. The time-dependent Euler angles (boxed), Ω_{LF-M1F} are modulated by the global motion. The distributed Euler angles (boxed), Ω_{VF-OF}, are associated with the local ordering. (B) Pictorial representation of the frames shown in part A, in the context of a typical protein structure. Note that in this figure the frames VF and M1F are separated. This corresponds to the general case, in which the global diffusion tensor, $\boldsymbol{D}_1$, with PAS M1F, is nonspherically symmetric. The Euler angles Ω_{OF-DF}, Ω_{OF-M2F}, and Ω_{DF-CF} in part a correspond to Ω_D, Ω_O, and Ω_{DC}, respectively, in part B.

dependent Euler angles are Ω_{LF-VF} for the global motion and Ω_{VF-OF} for the local motion. The frames OF, M2F, DF, and CF are site-specific. The Euler angles Ω_{OF-DF}, Ω_{OF-M2F}, and Ω_{DF-CF} in Figure 2A correspond to Ω_D, Ω_O, and Ω_{DC}, respectively, in Figure 2B.

The local motion is described by a relative (probe versus protein) coordinate scheme. That is, $\Omega_{M1F-OF}(t) = \Omega_{LF-OF}(t) - \Omega_{LF-M1F}(t)$,[32−34] with the angles $\Omega_{LF-OF}(t)$ representing the combined rotations represented by $\Omega_{LF-M1F}(t)$ and $\Omega_{M1F-OF}(t)$. Each axial rotator when uncoupled is associated with three decay constants, $(\tau^K)^{-1} = 6D_\perp + K^2(D_\parallel - D_\perp)$, $K = 0, 1, 2$, where D stands for either D_1 or D_2.

In the current application of SRLS to NMR spin relaxation in proteins, the $\boldsymbol{D}_1$ rotator represents the global motion of the protein and the $\boldsymbol{D}_2$ rotator represents the local motion of the spin-bearing probe.[32−34] In this study, $\boldsymbol{D}_1$ is taken isotropic and $\boldsymbol{D}_2$ is allowed to be to axially symmetric. Thus, the global motion is described by the correlation time $(\tau^0)^{-1} = 6D_1$ corresponding to $K = 0$, where D_1 is the eigenvalue of the $\boldsymbol{D}_1$ tensor. On the other hand, the local motion is described by three decay constants, $(\tau^K)^{-1}$, $K = 0, 1, 2$, that depend (as outlined generally in the previous paragraph) on the eigenvalues of the $\boldsymbol{D}_2$ tensor, $D_{2,\parallel}$ and $D_{2,\perp}$. One may also define $\tau_{2,\parallel} = 1/(6D_{2,\parallel})$ and $\tau_{2,\perp} = 1/D_{2,\perp}$; these correlation times are used in the present study.

The two rotators are coupled by the potential of mean torque (POMT), $U(\Omega_{VF-OF})$, where VF is the local director and OF is the local ordering frame. In general, the potential is expanded in the full basis set of the Wigner rotation matrix elements. When only the $L = 2$ terms are preserved, one has[32−34]

$$u(\Omega_{VF-OF}) = \frac{U(\Omega_{VF-OF})}{k_B T} \approx -c_0^2 D_{00}^2(\Omega_{VF-OF}) - c_2^2[D_{02}^2(\Omega_{VF-OF}) + D_{0-2}^2(\Omega_{VF-OF})] \quad (1)$$

The coefficient c_0^2 evaluates the strength of the POMT, and c_2^2 its nonaxiality.

The local order parameters are defined as[32−34]

$$\langle D_{0m}^2(\Omega_{VF-OF})\rangle = [\int d\Omega_{VF-OF}\, D_{0m}^2(\Omega_{VF-OF}) \exp[-u(\Omega_{VF-OF})] / [\int d\Omega_{VF-OF} \exp[-u(\Omega_{VF-OF})] \quad (2)$$

For at least 3-fold symmetry around the local director and at least 2-fold symmetry around the Z-axis of the local ordering frame, only $S_0^2 \equiv \langle D_{00}^2(\Omega_{VF-OF})\rangle$ and $S_2^2 \equiv \langle D_{02}^2(\Omega_{VF-OF}) + \langle D_{0-2}^2(\Omega_{VF-OF})\rangle$ survive.[21] The Saupe scheme order parameters relate to S_0^2 and S_2^2 as $S_{xx} = ((3/2)^{1/2} S_2^2 - S_0^2))/2$, $S_{yy} = -((3/2)^{1/2} S_2^2 - S_0^2))/2$ and $S_{zz} = S_0^2$.[32,33] In this study, we assume that 3-fold symmetry also prevails around the Z-axis of the local ordering frame. In this case, the second term on the right of eq 1 is zero, and $S_2^2 = 0$.

Here, the local motion is diffusive. Infrequent jumps among potential wells, with diffusive motion within the wells, can be modeled by properly designing the POMT$_1$.[20]

The Boltzmann distribution is $8\pi^2 P_{eq} = \exp[-U(\Omega_{VF-OF})/k_B T]/\langle\exp[-U(\Omega_{VF-OF})/k_B T]\rangle$, where $\langle ...\rangle$ means averaging over Ω_{VF-OF}.

The Smoluchowski equation for the coupled system is given by[32−34]

$$\frac{\partial}{\partial t} P(X, t) = -\hat{\Gamma} P(X, t) \quad (3)$$

where X is a set of coordinates completely describing the system. One has

$$X = (\Omega_{VF-OF}, \Omega_{LF-VF}),$$
$$\hat{\Gamma} = \hat{J}(\Omega_{VF-OF})\mathbf{D}_2 P_{eq} \hat{J}(\Omega_{VF-OF})(P_{eq})^{-1} + [\hat{J}(\Omega_{VF-OF} - \hat{J}(\Omega_{LF-VF}))]\mathbf{D}_1 P_{eq} [\hat{J}(\Omega_{VF-OF}) - \hat{J}(\Omega_{LF-VF})](P_{eq})^{-1}, \quad (4)$$

where $\hat{J}(\Omega_{VF-OF})$ and $\hat{J}(\Omega_{LF-VF})$ are the angular momentum operators for the probe and the protein, respectively. Note that$\Omega_{LF-VF} = \Omega_{LF-M1F} + \Omega_{M1F-VF}$. (That is, Ω_{LF-VF} represents the combined effects of rotations by both sets of Euler angles

dx.doi.org/10.1021/jp301999n | J. Phys. Chem. B 2012, 116, 6118−6127

on the right of this equation, where Ω_{M1F-VF} is time-independent).

Equation 3 is solved to yield the SRLS time correlation functions that lead by Fourier transformation to the spectral densities, $j_{K,K'}(\omega) = \Sigma_i(c_{K,K',i}\tau_i)/(1 + \omega^2\tau_i^2)$.[32−34] In practice, a finite number of terms is sufficient for numerical convergence of the solution. The $j_{K,K'}(\omega)$ functions are assembled into measurable spectral densities according to the local geometry (e.g., see chapter 12 of ref 49). For N−H bond dynamics, the relevant measurable spectral densities are J^{DD} for the $^{15}N-^{1}H$ dipolar interaction and J^{CC} for the ^{15}N CSA interaction. J^{DD} depends on the Euler angles Ω_{OF-DF} whereas $J^{CC}(\omega)$ depends on the Euler angles Ω_{OF-DF} and Ω_{DF-CF}. Note that the derivation of $J^{CC}(\omega)$ invariably requires the spectral densities $j_{11}(\omega)$ and $j_{22}(\omega)$ in addition to $j_{00}(\omega)$; $j_{11}(\omega)$ and $j_{22}(\omega)$ are unavailable in MF.

Cross-correlated spin relaxation,[50−52] featuring $J^{XY}(\omega)$, is treated in complete analogy with autocorrelated spin relaxation. The calculation of $J^{DC}(\omega)$ from the $J_{KK'}(\omega)$ functions is based on the Wigner rotation $R(\Omega_{OF-DF})$ followed by the Wigner rotation $R(\Omega_{DF-CF})$.

For rhombic local ordering and axial (e.g., dipolar) magnetic interaction six distinct pairs, $K,K' = (0,0)$, $(1,1)$, $(2,2)$, $(0,2)$, $(-1,1)$ and $(-2,2)$, have to be considered. For axial local ordering, assumed in this study, only the components $K,K = (0,0)$, $(1,1)$ and $(2,2)$ have to be considered (reducing significantly the computational effort). In this case, the explicit expression for $J^{DD}(\omega)$ is

$$J^{DD}(\omega) = (d_{00}^2(\beta_{OF-DF}))^2 j_{00}(\omega) + 2(d_{10}^2(\beta_{OF-DF}))^2 j_{11}(\omega) + 2(d_{20}^2(\beta_{OF-DF}))^2 j_{22}(\omega) \quad (5)$$

The autocorrelated ^{15}N relaxation parameters T_1, T_2 and $^{15}N-\{^{1}H\}NOE$ are calculated as a function of $J^{DD}(0)$, $J^{DD}(\omega_H)$, $J^{DD}(\omega_N)$, $J^{DD}(\omega_H - \omega_N)$, $J^{DD}(\omega_H + \omega_N)$, $J^{CC}(0)$, $J^{CC}(\omega_N)$ and the magnetic interactions, using standard expressions for NMR spin relaxation.[53−55] The cross-correlated relaxation rates associated with N−H bond dynamics, η_z and η_{xy},[52] feature the measurable spectral density, $J^{DC}(\omega)$, obtained as outlined above, and the $^{15}N-^{1}H$ dipolar/^{15}N CSA magnetic interaction cross-term.

Our most recent fitting scheme for SRLS[34] allows (among other enhancements) separating the local ordering and the local diffusion tensor frames. This feature is used in the present study. We call the software package developed in ref 34 C++OPPS (coupled protein probe Smoluchowski). It is available at the Web site http://www.chimica/unipd.it/licc/software.html, and described in detail in ref 34.

The parameter combination appropriate for analyzing given experimental data is determined by requiring good correspondence between theory and experiment, internal consistency, and physical tenability of the results. The tensorial representation makes it possible to materialize realistic geometry and tensor symmetry. For typical data sets comprising six data points − ^{15}N T_1, T_2, and $^{15}N-\{^{1}H\}$ *NOE* acquired at two magnetic fields − allowing D_2, c_0^2, c_2^2 and β_{OF-DF} to vary was found to be appropriate.[32,33] The starting value of β_{OF-DF} was taken as −101.3°, which is the standard angle between N−H and $C_{i-1}^{\alpha}-C_i^{\alpha}$ (e.g., see ref 43).

In this study, we allow $D_{2,\|}$, c_0^2, $D_{2,\perp}$, β_{OF-DF}, and β_{OF-M2F} to vary. The starting value of $D_{2,\perp}$, which represents backbone motion, is D_1. The starting value of β_{OF-DF} is −101.3° (see above). The starting value of β_{OF-M2F} is −101.3°; in the SRLS frame structure this sets the principal axis of the local diffusion tensor parallel to the N−H bond, in agreement with $D_{2,\|}$ representing N−H fluctuations.

2.2. Model-Free. The MF approach gives directly the measurable spectral density $J(\omega) = J^{DD}(\omega) = J^{CC}(\omega)$, made up of two Lorentzian terms that represent the global motion, and a single (effective) local motion.[28,29] This simple form is based on the premise that these dynamic processes are statistically independent by virtue of being time scale separated.[28] All the tensorial properties are simple: the global diffusion is isotropic, the local motion is isotropic, the local ordering is axial and its principal axis is collinear with the principal axis of the collinear axial magnetic tensors involved. Under these circumstances, the MF spectral density is given by:[28]

$$J(\omega) = S^2\tau_m/(1 + \tau_m^2\omega^2) + (1 - S^2)\tau_e^{|}/(1 + \tau_e^{|2}\omega^2) \quad (6)$$

The parameter τ_m is the correlation time for global motion, and $\tau_e \ll \tau_m$ is the effective correlation time for local motion. By virtue of $\tau_e \ll \tau_m$, one has $1/\tau_e^{|} = 1/\tau_m + 1/\tau_e \sim 1/\tau_e$. S^2 is defined as the plateau value, $C^L(\infty)$, to which the local motional time correlation function, $C^L(t)$, converges at long times. $C^L(\infty)$ is given by $(4\pi/5)^2 \Sigma_{m=0,\pm1,\pm2} |\langle Y_{2m}(\theta,\varphi)\rangle\langle Y_{2m}^*(\theta,\varphi)\rangle|$, where Y_{2m} are the spherical harmonics of Brink and Satchler.[56] The "generalized" order parameter is defined as $S \equiv (C^L(\infty))^{1/2}$.[28] S^2 is considered to represent the amplitude of the local motion. This interpretation is physically appropriate when the POMT is axial and strong, and the local motion is so fast as to be completely averaged out.[21] On the basis of the theory of moments, τ_e is defined as the area of the exact time correlation function for internal motion (corresponding to a "frozen" protein[28]) divided by $(1 - S^2)$.

The MF spectral density of ref 28 was obtained in ref 57 as the solution of the two-body SRLS Smoluchowski equation in the simply limit specified above.

The extended MF (EMF) spectral density is given by[30]

$$J(\omega) = S_f^2[S_s^2\tau_m/(1 + \omega^2\tau_m^2) + (1 - S_s^2)\tau_s^{|}/(1 + \omega^2\tau_s^{|2})] + (1 - S_f^2)\tau_f^{|}/(1 + \omega^2\tau_f^{|2}) \quad (7)$$

The parameter τ_f ($\tau_f^{|}$) is the (effective) correlation time for fast local motion. The parameter τ_s ($\tau_s^{|}$) is the (effective) correlation time for slow local motion. S_s^2 and S_f^2 are squared generalized order parameters associated with these motions. One has $1/\tau_f^{|} = 1/\tau_f + 1/\tau_m \sim 1/\tau_f$ and $1/\tau_s^{|} = 1/\tau_s + 1/\tau_m$. The large time scale separation assumption underlying eq 7 (ref 30) requires that $\tau_f^{|} \ll \tau_m$ and $\tau_s^{|} \ll \tau_m$. Yet, the EMF formula is used typically when $\tau_s^{|}$ and τ_m occur on the same time scale. The third term of eq 7 is often omitted under the assumption that $\tau_f^{|}$ is very small, obtaining thereby the reduced EMF formula.

The EMF spectral density was obtained in ref 58 as the measurable spectral density of a simple solution of the two-body Smoluchowski equation. This solution is valid in the limit of large time scale separation, rhombic local ordering, axial local diffusion and a 90° tilt between the main axis of the local ordering tensor and the principal axis of the axial magnetic tensor(s).

Analytical model-free time correlation functions, considered more general, have also been suggested. Their generality is substantiated through physically vague constructs.[59]

dx.doi.org/10.1021/jp301999n | J. Phys. Chem. B 2012, 116, 6118−6127

3. RESULTS AND DISCUSSION

The experimental data used in this study were kindly provided by Prof. Lewis E. Kay of the University of Toronto; experimental details appear in ref 60. We describe below their analysis using MF (section 3.1) and SRLS (section 3.2).

3.1. MF analysis. Figure 3 shows the experimental data used in this study. They comprise ^{15}N T_1, T_2, and ^{15}N−{^{1}H}

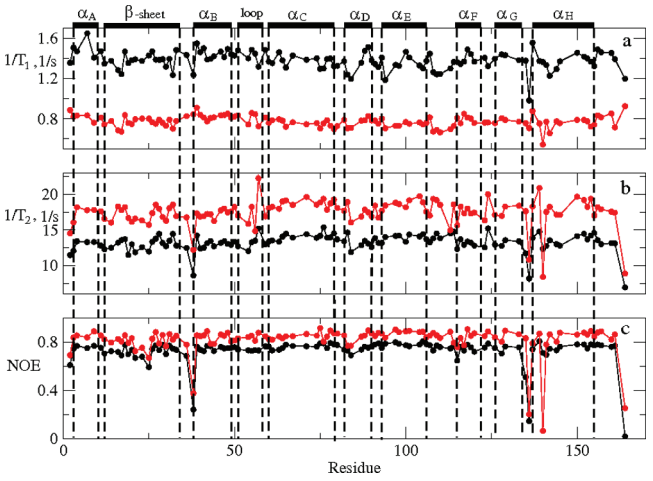

Figure 3. Experimental ^{15}N $1/T_1$ and $1/T_2$ and ^{15}N−{^{1}H} *NOE* relaxation parameters acquired at 11.7 (black) and 18.8 (red) T, and 298 K. The experimental methodologies used are described in ref 60. Prof. Lewis E. Kay of the University of Toronto kindly provided these data. The errors are generally on the order of 2%. The errors in the ^{15}N−{^{1}H}*NOE*s are in some cases 3%.

NOE acquired at 11.7 and 18.8 T, and 298 K. Using the computer program "quadric"[61,62] and the 3LZM crystal structure,[4,5] we determined (according to the standard procedure) the global diffusion tensor, $\boldsymbol{D}_1$. This analysis yielded an axial tensor with $D_{1,\mathrm{iso}} = 1.46 \times 10^7$ s^{-1}, $D_{1,\parallel}/D_{1,\perp} = 1.32$, $\Theta = 29.2°$ and $\Phi = 14.9°$ (the angles Θ and Φ describe the orientation of the principal axis of $\boldsymbol{D}_1$ in the inertia tensor frame of the crystal structure). As pointed out above, there is ample evidence for fast conformational interconversion in solution among open and closed T4L conformations.[5,8−10] Similar scenarios were encountered previously with other multidomain proteins. In those cases, the global diffusion tensor was found to be on average isotropic.[35,36,63] Given that ref 11 reported on an average solution structure that is more open than 3LZM, we examine below the effect of $\boldsymbol{D}_1$ axiality on the analysis.

The MF-based computer program "dynamics",[64] which features models 1−4 based on the MF formula (eq 6), and models 5−8 based on the EMF formula (eq 7), was used to fit the data shown in Figure 3. In this fitting scheme, the parameter S^2 is allowed to vary in model 1. S^2 and τ_e are allowed to vary in model 2. S^2 and the conformational exchange term, R_{ex} (S^2, τ_e, and R_{ex}) are allowed to vary in model 3 (4). S_s^2, S_f^2, and τ_s (S_s^2, S_f^2, τ_s and τ_f) are allowed to vary in model 5 (6). S_s^2, S_f^2, τ_s and R_{ex} (S_s^2, S_f^2, τ_s, τ_f and R_{ex}) are allowed to vary in model 7 (8). The fitting process starts with model 1, which is enhanced as required to more complex models, according to standard statistical criteria.

The results of applying "dynamics" to the two-field data set of Figure 3 are shown in Figure 4 for isotropic global diffusion with $D_1 = 1.46 \times 10^7$ s^{-1} (black), and axial global diffusion

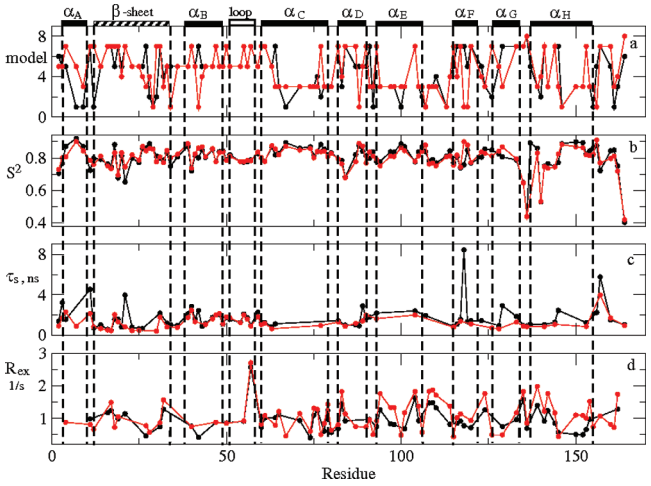

Figure 4. Best-fit values of the squared generalized order parameter, S^2 (b), the correlation time for slow local motion, τ_s (c), and the conformational exchange term, R_{ex} (d), obtained by fitting the data shown in Figure 3 with the computer program "dynamics"[55] for an isotropic (black) or axially symmetric (red) global diffusion tensor, $\boldsymbol{D}_1$. Part a shows the model selected for each N−H bond. The isotropic global diffusion tensor used has $D_1 = 1.46 \times 10^7$ s^{-1}. The axial global diffusion tensor, determined with the computer program "quadric",[52] has $D_{1,\mathrm{iso}} = 1.46 \times 10^7$ s^{-1}, $D_{1,\parallel}/D_{1,\perp} = 1.32$, $\Theta = 29.2°$, and $\Phi = 14.9°$. Values of $r_{HN} = 1.02$ Å and $\Delta\sigma = -170$ ppm were used for the N−H bond length and ^{15}N chemical shift anisotropy (CSA), respectively.

(using the tensor given above) (red). The model selection is illustrated in Figure 4a. It can be seen that using axial instead of isotropic $\boldsymbol{D}_1$ implies primarily an interchange of models 1 and 3, or models 5 and 7, with an increase in the overall number of R_{ex} terms. Corresponding S^2 and τ_s values are quite similar, except for several cases where τ_s is larger and S^2 is smaller for isotropic $\boldsymbol{D}_1$ (Figures 4b,c).

For isotropic (axial) $\boldsymbol{D}_1$ tensor, 52% (66%) of the N−H bonds feature R_{ex} terms. The latter represent 7.1% of ^{15}N $1/T_2$ at 11.7 T and 14.6% of ^{15}N $1/T_2$ at 18.8 T. The average error in the experimental ^{15}N $1/T_2$ values is 2%. Thus, the R_{ex} contribution to the transverse relaxation rate is significant. In many cases, the R_{ex} term is larger for axial $\boldsymbol{D}_1$. The single-field data sets (respective results not shown), and the two-field data set, yield different patterns and absolute values of R_{ex}. Conformational exchange in T4L has not been confirmed by independent relaxation dispersion experiments.

The R_{ex} terms are not reduced substantially (rather, their number has increased significantly) by using axial instead of isotropic $\boldsymbol{D}_1$, as one would expect had they arisen from having absorbed $\boldsymbol{D}_1$ axiality. The best-fit MF parameters, S^2 and τ_s (also S_f^2, not shown), are largely the same for isotropic and axial $\boldsymbol{D}_1$. These findings imply that the R_{ex} terms emerge largely from force-fitting the experimental data, i.e., from calculations where the statistical criteria are fulfilled but the best-fit parameters are inaccurate, having absorbed unaccounted for factors. Clearly, these factors are associated with features other than $\boldsymbol{D}_1$ axiality. To identify them, we carry out SRLS analysis (see below), and compare the two analyses.

In Figure 5 we show the best-fit MF parameters in a form that allows comparison with the SRLS results. We used axial $\boldsymbol{D}_1$, although very similar results (not shown) are obtained with isotropic $\boldsymbol{D}_1$. Figure 4a indicates that the fitting procedure determined predominantly models 5 and 7 for the N-terminal

dx.doi.org/10.1021/jp301999n | J. Phys. Chem. B 2012, 116, 6118−6127

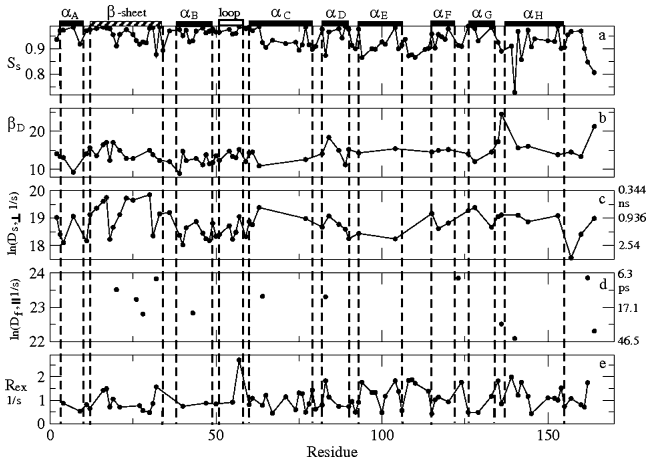

Figure 5. Best-fit values of the order parameter for slow local motion, S_s (a). The angle $\beta_D \equiv \beta_{OF-DF}$ calculated from the relation $S_f^2 = (d_{00}^2(\beta_{OF-DF}))^2 = (1.5\ \cos^2(\beta_{OF-DF}) - 0.5)^2$ (b). The natural logarithm of the rate of slow local motion, $D_s = 1/(6\tau_s)$, given in s^{-1}; τ_s is given on the right in *ns* (c). The natural logarithm of the rate of fast local motion, $D_f = 1/(6\tau_f)$, given in s^{-1}; τ_f is given on the right in *ps* (d). The conformational exchange term, R_{ex} (e). An axial global diffusion tensor with $D_{1,iso} = 1.46 \times 10^7\ s^{-1}$, $D_{1,\|}/D_{1,\perp} = 1.32$, $\Theta = 29.2°$ and $\Phi = 14.9°$ was used. The program "dynamics"[64] was used to fit the experimental data shown in Figure 3. The abscissa represents the protein sequence. The errors are estimated at 3%.

domain, model 3 for the linker, and models 3 and 7 for the C-terminal domain.

Figure 5a shows the parameter S_s. The spectral density of eq 7 is formally analogous to eq B6 of ref 58; S_s is formally analogous to the axial order parameter, S_0^2, in that equation. S_0^2 is a measure of ordering strength. Thus, S_s has a clear physical meaning provided it has virtually the same value as S_0^2. To determine the relation between the generalized order parameter (S) and S_0^2, we recall the definition $S^2 = \Sigma_{m=0,\pm1,\pm2} |\langle D_{0m}^2\rangle\langle D_{0-m}^2\rangle|$ from ref 28, given in section 2.2. S^2 may be calculated in any frame. In the PAS of the local ordering tensor, where only $\langle D_{00}^2\rangle$ and $\langle D_{02}^2 + D_{0-2}^2\rangle$ survive, one has

$$S^2 = \langle D_{00}^2\rangle^2 + 2\{\mathrm{Re}\langle D_{02}^2\rangle\}^2 \quad (8)$$

Given that $S_0^2 = \langle D_0^2\rangle$ and $S_2^2 = \langle D_{02}^2 + D_{0-2}^2\rangle = 2\{\mathrm{Re}\langle D_{02}^2\rangle\}$, one has:

$$S^2 = (S_0^2)^2 + \frac{1}{2}(S_2^2)^2 \quad (9)$$

Thus, S evaluates the strength of the local ordering when $S_2^2 = 0$, provided that S and S_0^2 are virtually the same.

The MF analysis yielded average S_s values of 0.96, 0.935, and 0.93 for the N-terminal domain, the C-terminal domain, and the linker (Figure 5a). Thus, according to MF, the weakest ordering prevails in the linker. Figure 5b shows the parameter S_f^2 converted into the angle $\beta_D = \beta_{OF-DF}$ according to $S_f^2 = (1.5\ \cos\beta_D^2 - 0.5)^2$. This relation is based on the formal analogy between the reduced EMF formula (eq 7 with $\tau_s^{-1} = 0$), and the truncated form of eq 5 where the second and third terms are omitted, and $j_{00}(\omega)$ is given by eq 6. Comparison between the two expressions reveals that $S_f^2 = (d_{00}^2(\beta_{OF-DF}))^2 = (1.5\ \cos\beta_D^2 - 0.5)^2$.[31,32] β_D is a geometric parameter associated with a frame transformation;[31,32] it should not be associated with an order parameter.[30] In this case, the angle β_D represents the deviation of Z_{OF}, the principal axis of the local ordering tensor from Z_{DF}, the principal axis of the dipolar tensor (which points along the N−H bond). Most β_D angles are in the 12−17° range.

Note that the reduced EMF formula, which underlies models 5 and 7, is problematic. The coefficients of the terms in a physical spectral density sum up to 1. Mere elimination of the third term of eq 7 leads inherently to force-fitting because the best-fit parameters absorb the effect of the omitted term.[32,33] Simplifications should be made by designing the appropriate form of the Markov operator in the Smoluchowski equation.[32,33]

Figure 5c shows the natural logarithm of $1/(6\tau_s)$, with τ_s given in seconds. The slow local motional correlation time, τ_s corresponds formally to $\tau_{2,\perp} = (1/6D_{2,\perp})$.[32] τ_s varies (approximately) between 0.35 and 3.5 ns. Figure 5d shows the natural logarithm of $1/(6\tau_e)$ or $1/(6\tau_f)$, with τ_e and τ_f given in seconds (τ_e is defined in the context of eq 6). τ_f and τ_e correspond formally to $\tau_{2,\|} = (1/6D_{2,\|})$,[32] which represents N−H bond vector fluctuations. For most N−H bonds, τ_f and τ_e are zero.

Figure 5e shows the R_{ex} term. This parameter was discussed in the context of Figure 4a.

3.2. SRLS analysis. Using the axial global diffusion tensor, $\boldsymbol{D_1}$, given in the first paragraph of section 3.1, and typical local motional parameters obtained with the SRLS analysis (see below), we calculated ^{15}N T_1, T_2 and $^{15}N-\{^1H\}$ *NOE* for angles, β_{M1F-VF}, of 0° and 90° between the principal axis of the global diffusion tensor, Z_{M1F}, and the local director, VF (i.e., the average orientation of the N−H bond). The differences between corresponding relaxation parameters evaluate the maximum effect $\boldsymbol{D_1}$ axiality has on the analysis. We obtained −5.0% for ^{15}N T_1, 5.2% for ^{15}N T_2, and 0.6% for the $^{15}N-\{^1H\}$ *NOE*, for a magnetic field of 14.1 T. These differences are small. For most N−H bonds, the angle β_{M1F-VF} differs from 90°; in these cases, the differences are even smaller. On the basis of these results, and the related evidence presented in section 3.1, we take the $\boldsymbol{D_1}$ tensor as isotropic with $D_1 = 1.46 \times 10^7\ s^{-1}$.

Figure 6 shows the best-fit parameters obtained by fitting with SRLS the experimental data shown in Figure 3. Figure 7 shows the average best-fit parameters for the various secondary structure elements and loops. The purpose of this figure is to identify tensorial local ordering and local diffusion features characteristic of given elements of secondary structure, or loops. Figure 8 shows the average best-fit parameters for the N-terminal domain, the C-terminal domain, and the linker. The purpose of this figure is to delineate differences and similarities among the N-terminal domain, the C-terminal domains, and the linker in terms of the principal values and orientation of the $\boldsymbol{S}$ and $\boldsymbol{D_2}$ tensors.

As pointed out above, we analyze the restricted local motion at the N−H sites of T4L in terms of rank 2 local ordering and local diffusion tensors. The data shown in Figures 6−8 represent the principal values and orientations of these tensors.

The principal value, S_0^2, of the local ordering tensor, $\boldsymbol{S}$, is shown in Figure 6a. Most N−H bonds have $S_0^2 = 0.91 \pm 0.046$. The error is 5% of the absolute value. It has been increased beyond the determined 3% error (see below), because in the limit of strong ordering large changes in c_0^2 (which is varied in the data-fitting process) correspond to very small changes in $(S_0^2)^2$ (cf. Figure 4 of ref 32), hence also S_0^2. Sporadic smaller (larger) S_0^2 values appear in the β-sheet, the α_D helix, and the α_E/α_F loop (the C-terminal chain segment, the α_B/α_C loop and the α_H helix). The average S_0^2 values shown in Figure 7a are

dx.doi.org/10.1021/jp301999n | J. Phys. Chem. B 2012, 116, 6118−6127

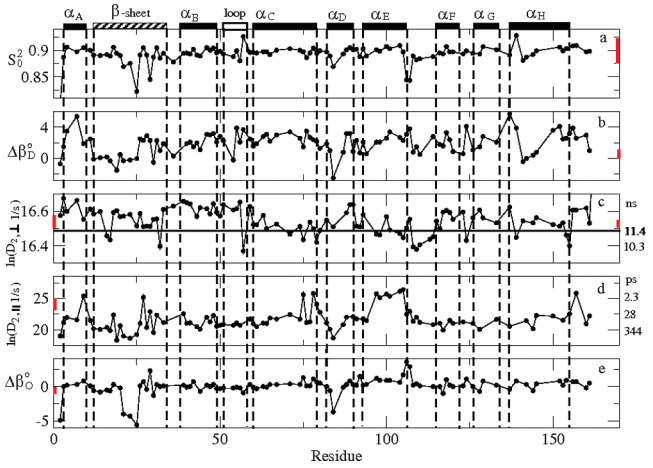

Figure 6. Best-fit values of the principal value of the local ordering tensor (i.e., the order parameter), S_0^2 (a). The deviation of the principal axis of the local ordering tensor from the $C_{i-1}^{\alpha}-C_i^{\alpha}$ axis, $\Delta\beta_D$ (b). The natural logarithm of the perpendicular component of the local diffusion tensor, $D_{2,\perp}$, given in s^{-1}; $\tau_{2,\perp} = 1/(6D_{2,\perp})$ is shown on the right in *ns* (c). The natural logarithm of the parallel component of the local diffusion tensor, $D_{2,\parallel}$, given in s^{-1}; $\tau_{2,\parallel} = 1/(6D_{2,\parallel})$ is shown on the right in *ps* (d). The deviation of the principal axis of the local diffusion tensor from the N−H bond, $\Delta\beta_O$ (e). We used isotropic global diffusion tensor with $D_1 = 1.46 \times 10^7$ s^{-1}, $r_{HN} = 1.02$ Å for the N−H bond length, and $\Delta\sigma = -170$ ppm for the ^{15}N CSA. The experimental data shown in Figure 3 were used. The abscissa represents the protein sequence. The errors are estimated at 3%.

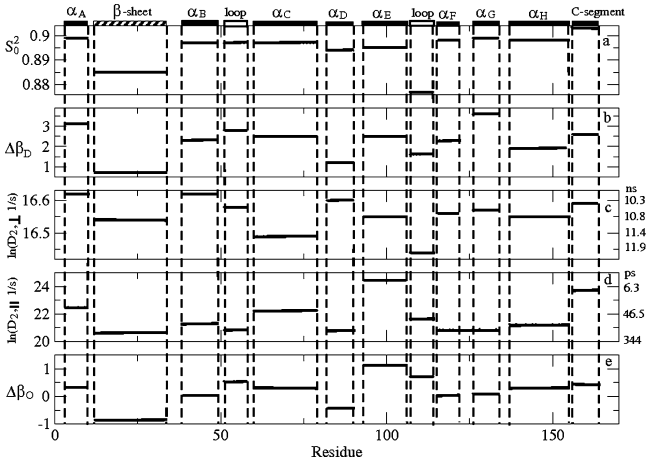

Figure 7. As in the captions of Figure 6, except that average best-fit values over the various secondary structure elements are shown.

mostly 0.91. The exceptions (appearing in the β-sheet and the C-terminal segment) deviate from 0.91 by less than 2%; this is within the experimental error. As expected, the average S_0^2 values shown in Figure 8a are also within the experimental error. It may be concluded that strong and largely constant local ordering prevails at the N−H sites of T4L.

The orientation of the local ordering tensor, **S**, is represented by the angle $\Delta\beta_D$, shown in Figure 6b. As pointed out above, at the start of the fitting process the principal axis of **S**, Z_{OF}, is set along the $C_{i-1}^{\alpha}-C_i^{\alpha}$ axis. Thus, the best-fit value of $\Delta\beta_D$ measures the deviation of Z_{OF} from this axis. The extreme values of $\Delta\beta_D$ are −2° and 6°. On average, $\Delta\beta_D$ is nearly zero in the first half of the β-sheet and nearly 2° in its second part. Relatively large variations in $\Delta\beta_D$ are featured by the α_B/α_C loop and the α_D and α_H helices. $\Delta\beta_D$ is approximately 2.5° throughout the α_C helix.

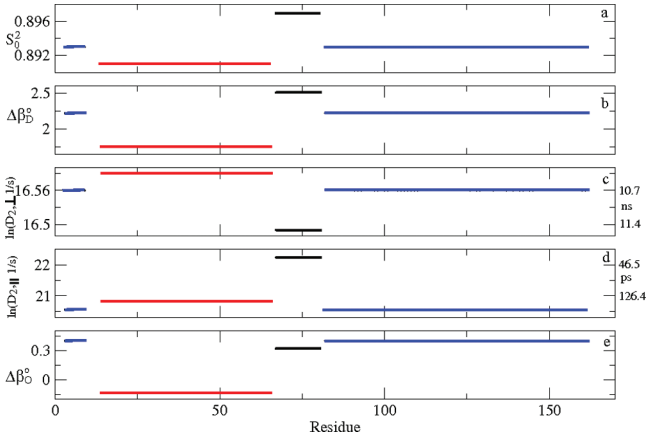

Figure 8. As in the captions of Figure 6, except that average best-fit values over the N-terminal domain (red), the linker (black), and the C-terminal domain (blue) are shown.

The smallest (largest) average $\Delta\beta_D$ value is found in the β-sheet (α_G helix); in general, the $\Delta\beta_D$ pattern is quite diversified (Figure 7b). Figure 8b shows that for the N-terminal (C-terminal) domain, Z_{OF} is virtually parallel to $C_{i-1}^{\alpha}-C_i^{\alpha}$ (deviates from $C_{i-1}^{\alpha}-C_i^{\alpha}$ by 2.4°). The largest deviation, exceeding 2.5°, is observed for the linker. Differences on the order of 2.5° are significant. Although there is ample evidence for the local ordering at N−H sites in proteins being centered at $C_{i-1}^{\alpha}-C_i^{\alpha}$,[32−48] experimental-data-based quantification of this feature in terms of tensor orientation is new.

Figures 6c−e, 7c−e, and 8c−e illustrate the local diffusion tensor, $\boldsymbol{D_2}$. The natural logarithm of the perpendicular component, $D_{2,\perp}$ (given in units of s^{-1}) is shown in Figures 6c−8c; on the right of the ordinates, we show $\tau_{2,\perp} = 1/(6D_{2,\perp})$ in *ns*. $D_{2,\perp}$ may not be smaller than the global diffusion rate of $D_1 = 1.46 \times 10^7$ s^{-1}. The solid line in Figure 6c corresponds to $\ln(D_1\ s^{-1})$. A few $\ln(D_{2,\perp}\ s^{-1})$ values are approximately 10% smaller than $\ln(D_1\ s^{-1})$; in these cases, the SRLS model appears to be too simple.

The average values of $D_{2,\perp}$, shown on a logarithmic scale in Figure 8c, are 1.62×10^7, 1.56×10^7, and 1.46×10^7 s^{-1} for the N-terminal domain, the C-terminal domain and the linker. Converting these rates into average correlation times, $\tau_{2,\perp}$, one obtains 10.3, 10.7, and 11.4 ns, respectively. The error in the correlation time for global motion, $\tau_m = 11.4$ ns, is ±0.3 ns. Thus, the differences between the $\tau_{2,\perp}$ values for the mobile domains and the linker are significant.

Figures 6d−8d show the natural logarithm of the parallel component of the local diffusion tensor, $D_{2,\parallel}$. This dynamic mode is associated with N−H fluctuations around the equilibrium N−H orientation. On the right of the ordinates of Figures 6d−8d we show the corresponding correlation times, $\tau_{2,\parallel} = 1/(6D_{2,\parallel})$. The smallest (largest) $D_{2,\parallel}$ values are found in the β-sheet and the α_D helix (the α_E helix and at several sporadic positions along the polypeptide chain). Ignoring the outliers, an average value of 125 ps is obtained. This is a reasonable value, consistent with MD/ED-based information on local bond-vector fluctuations in proteins, in general,[65] and T4L, in particular.[8] Figure 8d shows the N−H fluctuations in the N-terminal domain, the C-terminal domains, and the linker. They occur at average rates of 1.3×10^9, 1.8×10^9 and (excluding the α_E helix) 5.3×10^9 s^{-1}, respectively. Thus, in the

dx.doi.org/10.1021/jp301999n | J. Phys. Chem. B 2012, 116, 6118−6127

N-terminal (C-terminal) domain the N−H bonds fluctuate 4.1 (2.9) times faster than in the linker.

The orientation of the local diffusion tensor, $\boldsymbol{D_2}$, is given by the angle $\Delta\beta_O$, which represents the deviation of its principal axis, Z_{M2F}, from the N−H bond (Figure 6e). $\Delta\beta_O$ is virtually zero for most of the N−H bonds of T4L. Exceptional $\Delta\beta_O$ and $D_{2,\|}$ values (Figure 6d) require further investigation. The α_E helix is altogether an outlier (Figures 6d,e); it should also be studied further.

The overall picture concurs with collective reorientation of the peptide-bond planes within the N-terminal domain, and within the C-terminal domain. Collectivity is inferred based on similar local ordering and local diffusion parameters. These motions occur in the presence of spatial restrictions centered at the $C^{\alpha}_{i-1}-C^{\alpha}_i$ axes. Their rates ($D_{2,\perp}$) are somewhat faster than the rate of global tumbling (D_1). Recall, however, that SRLS (and its MF limit) is a mesoscopic approach. Both the local ordering and the local diffusion tensors are to be viewed as effective quantities, to which several different microscopic constituents might contribute (see section 3.3 below for a brief discussion of the SRLS/ESR analysis of local nitroxide motion). Ordering and motion around the $N_i-C^{\alpha}_i$, $C^{\alpha}_i-C_i'$, and $C^{\alpha}_{i-1}-C_{i-1}'$ bonds are potential candidates. The SRLS analysis is very sensitive to the local geometry. It can exclude predominance of given contributions. For example, let us consider the possibility that local ordering and local diffusion occur predominantly around the $N_i-C^{\alpha}_i$ bond. In this case, the best-fit value of β_D should have been near −119°.[69] In the extensive exploration of the vicinity of $\beta_D = -101.3°$, consistent convergence to $\beta_D = -119°$ was not observed.

The main local diffusion axis is in most cases virtually parallel to the N−H bond (Figure 6e). This geometric feature allows interpreting the parallel local diffusion rate, $D_{2,\|}$, as N−H bond-vector fluctuations and generally the perpendicular local diffusion rate, $D_{2,\perp}$, as backbone motion.

T4L samples labeled with (1-oxy-2,2,5,5,-tetramethylpyrrolinyl-3-methyl)-methanethiosulfonate at residue N72, which resides within the α_C helix, and residue V131, which resides within the α_G helix, were studied in ref 23 with SRLS/ESR. A local motional mode involving the nitroxide spin label and the α-helix housing it was detected at 22 °C. The respective rates are $3.3 \times 10^7$and 4.0×10^7 s^{-1} at 22 °C for the major (among several detected) conformations. The present SRLS/NMR study yielded $D_{2,\perp}$ of 1.62×10^7 and 1.56×10^7 s^{-1} for the N-terminal and C-terminal domains. The SRLS/NMR results are consistent with the SRLS/ESR results.

Error Estimation. MF analyses use experimental uncertainties within the scope of Monte Carlo-type strategies to evaluate errors in the best-fit parameters.[27] These procedures involve a large number of data-fitting calculations. The latter are feasible when the spectral densities are simple analytical functions, as in MF. They are (within the scope of acceptable statistics) impractical when they are obtained by solving numerically Smoluchowski equations, as in SRLS. Methods for error estimation not based on experimental uncertainties also have been reported in the literature. For example, the authors of ref 66 acquired 16 ^2H relaxation rates from $^{13}CH_2D$ methyl groups of ^{13}C-labeled, fractionally deuterated, B1 domain of peptostreptococcal protein L. All possible subsets comprising 14 relaxation rates were analyzed. The uncertainty in any given best-fit parameter was determined based on the ensuing variation in its value.

Here, the errors have been estimated varying the starting values of the variables in the fitting process. On average, this led to 3% error in all the variables. This result is viewed within the scope of the following earlier developments. In ref 67, we have shown that the parameter combination used herein − titled axial local ordering ($\boldsymbol{S}$) and local diffusion ($\boldsymbol{D_2}$) tensors − matches data sensitivity. In ref 68, we have shown that the global minimum can be attained when particular starting values, which represent a viable physical model that agrees with the stereochemistry of the peptide-bond plane, are used. They include $\beta_D = -101.3°$, implying that the principal axis of $\boldsymbol{S}$, Z_{OF}, is nearly parallel to the $C^{\alpha}_{i-1}-C^{\alpha}_i$ axis; $\beta_O = -101.3°$, implying that the principal axis of $\boldsymbol{D_2}$, Z_{M2F}, is nearly parallel to the N−H bond; and $D_{2,\perp} = D_1$, implying that the perpendicular local motional diffusion rate occurs on the same time scale as the global tumbling. On this basis, it was considered appropriate to estimate the errors in the best-fit parameters by varying c_0^2 in the 8−18 range, and $D_{2,\|}$ in the 10^9-10^{10} s^{-1} range.

In MF analyses the errors in the fast local motional correlation times, τ_e and τ_f, are typically much larger than the error in the global motional correlation time, τ_m. Here, and in SRLS analyses of other proteins,[67,68] the errors in $\tau_{2,\|}$ and $\tau_{2,\perp}$ are comparable to the error in τ_m. This feature is addressed below.

Let us consider the simple scenario called "model 2",[27,64] as applied to a spherical protein. MF determines τ_m based on ^{15}N T_1/T_2 data of N−H bonds considered "rigid". Using the emerging τ_m value, the complete ^{15}N relaxation data set is fit, allowing S^2 and τ_e to vary. In some cases, global optimization is carried out by varying τ_m. In most cases, τ_e does not exceed 50 ps; τ_m of medium-size proteins is in the 10−15 ns range. The error in τ_e is typically much larger than the error in τ_m; this is rationalized based on $\tau_e \ll \tau_m$. Similar considerations apply to τ_f in the context of "model 6" (defined in ref 64). SRLS fits the complete data set allowing c_0^2 (from which S_0^2 is calculated) and $\tau_2 = 1/(6D_2)$ to vary, for different values of τ_m. In the present case, the initial value of τ_m was determined with the computer program "quadric"[61] to be 11.4 ns. This parameter was then allowed to vary in the 10.9−11.9 ns range. The results were treated as illustrated in Figure 9 of ref 32, to find that the best-fit value is 11.4 ns.

The MF fitting scheme that determines τ_e is often underfitting the experimental data, impairing thereby the accuracy of the best-fit parameters, in particular the accuracy of $\tau_e \ll \tau_m$. The analogue of τ_e (which for wobble-in-a-cone in a square-well potentials depends on S^2 and the wobbling rate, D)[28,29] is $\tau_{ren} = 2\tau_2/c_0^2$ (τ_{ren} is the renormalized local motional correlation time discussed in detail in refs 32 and 33). The SRLS variable in the data-fitting process is τ_2 rather than τ_{ren}. For relatively rigid N−H bonds c_0^2 is on the order of 10−20.[32,33] Thus, τ_2 is 5−10 times larger than τ_e, implying a smaller time scale separation from τ_m. Hence, τ_2 is less vulnerable to eventual inaccuracies. Finally, in the present study, the local motion is axially symmetric. $\tau_{2,\perp}$ is comparable to τ_m. $\tau_{2,\|}$ is on average 128 and 93 ps for the N-, and C-terminal domains, respectively. It relates to τ_f by analogy with the relation of τ_2 to τ_e. This scenario differs substantially from the typical MF scenario described above. The matters pointed out in this paragraph are supportive of similar errors in τ_m, $\tau_{2,\|}$, and $\tau_{2,\perp}$.

3.3. The SRLS and MF Pictures. Figure 9a shows S_0^2 and its formal MF analogue, S_s. Clearly, they differ substantially within the scope of the error margins of the SRLS parameters, depicted on the right (black bars). The SRLS order parameter,

dx.doi.org/10.1021/jp301999n | J. Phys. Chem. B 2012, 116, 6118−6127

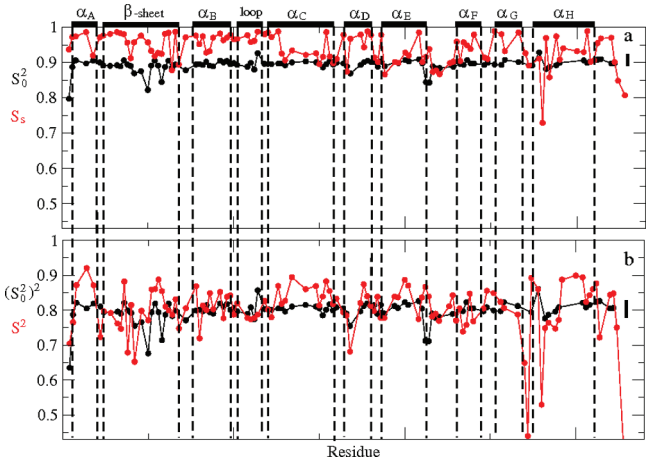

Figure 9. Axial SRLS order parameter, S_0^2 (black), and effective MF order parameter for slow local motion, S_s (red) (a) Squared axial SRLS order parameter, $(S_0^2)^2$ (black), and squared generalized MF order parameter, S^2 (red) (b). The abscissa represents the protein sequence. The errors in S_0^2 and $(S_0^2)^2$ are depicted on the right (black bars).

S_0^2, is on average 0.91, with several values in the 0.85−0.9 range. The relatively strong ordering reflected by these values is centered at the $C_{i-1}^{\alpha}-C_i^{\alpha}$ axis. This is consistent with crankshaft motions found with MD studies to dominate protein backbone dynamics, which are also centered at the $C_{i-1}^{\alpha}-C_i^{\alpha}$ axis.[48] The effective MF order parameter, S_s, is 0.92 for the linker, nearly 1 for many N−H bonds, and in all the cases larger than 0.9. The ordering is centered at an orientation tilted at 12−17° from the N−H bond. The unduly strong ordering in the N-, and C-terminal domains versus the weaker ordering in the linker, and an ordering axis tilted at 12−17° relative to the N−H bond, which cannot be associated with a feature of the 3D structure, are difficult to rationalize.

Figure 9b depicts S^2 and $(S_0^2)^2$. As shown above, $S^2 = (S_0^2)^2 + 0.5\,(S_2^2)^2$ (eq 9). The fact that S^2 differs significantly from $(S_0^2)^2$ indicates that the contribution of the rhombic term to S^2 is substantial. Thus, the composite S^2 has different meaning at the various N−H sites. SRLS determines (S_0^2) and β_D, which describe a well-defined rank 2 tensor, $\boldsymbol{S}$. The local ordering at the various N−H sites is characterized in terms of this tensor.

The SRLS analysis determines $\tau_{2,\perp}$ and $\tau_{2,\parallel}$ for every experimentally accessible N−H bond in T4L. Supported by the local geometry determined in this study, $\tau_{2,\perp}$ is interpreted as correlation time for collective domain motion, and $\tau_{2,\parallel}$ as correlation time for localized N−H bond vector fluctuations. $\tau_{2,\perp}$ is faster than the correlation time for global tumbling by approximately 10%. Such very slow (on the spin relaxation time scale) motion is consistent with the segmental movement of large domains (which constitute about 50% of the backbone), and in particular with the internal motion of the intricate C-terminal domain, which comprises the N-terminal α_A helix.

The local N−H bond-vector fluctuations, $\tau_{2,\parallel}$, are in the 30−125 ps range. The magnitude of $\tau_{2,\parallel}$ is consistent with MD studies.[65] The fact that $\tau_{2,\parallel}$ is 4.1 (2.9) times faster in the mobile domains than in the linker agrees with domain motion requiring significant internal structural rigidity, consistent with fast small-amplitude N−H fluctuations.

τ_s is on average 2 ns within the N-, and C-terminal domains (Figures 4c and 5c). For many N−H bonds, it is associated with nearly perfect ordering; this is difficult to rationalize. The large variations in τ_s (Figure 5c) are inconsistent with collective processes, usually associated with slow internal motions, which imply similar physical parameters of the pertinent N−H bonds. The correlation times, τ_e and τ_f, are zero for most N−H bonds (Figure 5d). As pointed out above, T4L exhibits substantial internal flexibility. There are specific reports on fast local motions, prevailing aside slow collective motions.[8] It is puzzling that the N−H bonds of T4L emerge in the MF analysis as largely "rigid" locally.

The SRLS analysis uses five well-defined variables − S_0^2 and β_D for the local ordering and $D_{2,\parallel}$, $D_{2,\perp}$, and β_O for the local diffusion. MF also uses five variables − S_s^2, S_f^2, τ_s, τ_f, and R_{ex}. The picture emerging from the SRLS parameters differs qualitatively from the picture emerging from the MF parameters.

4. CONCLUSIONS

^{15}N spin relaxation from T4 lysozyme is studied using the SRLS approach. The local motion is characterized in terms of tilted axial local ordering and local diffusion tensors. In the context of this description, and with mode-coupling accounted for, SRLS detects known catalysis-related domain motion. This process could not be detected in previous MF analysis of the same experimental data. The parameter that represents domain motion is the perpendicular component of the local diffusion tensor. The respective correlation times are 10.3 and 10.7 ns for the N-, and C-terminal domains; the correlation time for global tumbling is (11.4 ± 0.3) ns. The parallel component of the local diffusion tensor represents fast N−H bond vector fluctuations around the equilibrium N−H orientation. The correlation times for this motion are 128, 93, and 31 ps for the N-terminal domain, the C-terminal domain, and the interdomain linker. The local spatial restrictions at the N−H sites of T4L are strong and centered at the $C_{i-1}^{\alpha}-C_i^{\alpha}$ axis, as evidenced by the principal values and orientation of the local ordering tensors. The overall picture that emerges from the SRLS analysis concurs with collective peptide plane reorientation around $C_{i-1}^{\alpha}-C_i^{\alpha}$ as mechanism of domain motion. The standard tensorial perspective combined with an effective two-body coupled-rotator theory yielded an insightful picture of structural dynamics for T4L.

AUTHOR INFORMATION

Corresponding Author

*E-mail: meirove@biu.ac.il. Telephone: 972-3-531-8049. Fax: 972-3-738-4058.

Notes

The authors declare no competing financial interest.

ACKNOWLEDGMENTS

Prof. Lewis E. Kay of the University of Toronto, Toronto, Canada, is acknowledged gratefully for providing the experimental ^{15}N relaxation data from T4L, and for his interest in this work. Profs. Antonino Polimeno and Mirco Zerbetto of the University of Padova, Padova, Italy, are acknowledged for the development of the computer program C++OPPS, used in this study. This work was supported by the Israel Science Foundation (Grant No. 347/07 to E.M.), the Binational Science Foundation (Grant No. 2006050 to E.M. and Jack H. Freed), the German-Israeli Science Foundation for Scientific Research and Development (Grant No. 928-190.0/2006 to E.M. and Christian Griesinger of Max Planck Institute,

Göttingen, Germany), and the Damadian Center for Magnetic Resonance at Bar-Ilan University, Israel.

REFERENCES

(1) Streisinger, G.; Okada, Y.; Emrich, J.; Newton, J.; Tsugita, A.; Terzaghi, E.; Inouye, M. *Cold Spring Harbor Symp. Quant. Biol.* **1966**, *56*, 500.
(2) Tsugita, A. *In The Enzymes*, 3rd ed.; Boyer, P. D., Ed.; Academic Press: New York, 1971; Vol. *5*, pp 343−411.
(3) Columbus, L.; Kalai, T.; Jekö, J.; Hideg, K.; Hubbell, W. L. *Biochemistry* **2001**, *40*, 3828−3846.
(4) Weaver, L. H.; Matthews, B. W. *J. Mol. Biol.* **1987**, *193*, 189−199.
(5) Zhang, X.-J.; Wozniak, J. A.; Matthews, B. W. *J. Mol. Biol.* **1995**, *250*, 527−552.
(6) Bahar, I.; Erman, B.; Haliloglu, T.; Jernigan, R. L. *Biochemistry* **1997**, *36*, 13512−13523.
(7) Arnold, G. E.; Orenstein, R. L. *Proteins* **1994**, *18*, 19−33.
(8) de Groot, B. L.; Hayward, S.; van Aalten, D. M. F.; Amadei, A.; Berendsen, H. J. C. *Proteins* **1998**, *32*, 116−127.
(9) Mann, G.; Hermans, J. *J. Mol. Biol.* **2000**, *302*, 979−989.
(10) Zhang, Z.; Shi, Y.; Liu, H. *Biophys. J.* **2003**, *84*, 3583−3593.
(11) Goto, N. K.; Skrynnikov, N. R.; Dahlquist, F. W.; Kay, L. E. *J. Mol. Biol.* **2001**, *308*, 745−764.
(12) Najbar, L. V.; Craik, D. J.; Wade, J. D.; McLeish, M. J. *Biochemistry* **2000**, *39*, 5911−5920.
(13) Mchaourab, H. S.; Lietzow, M. A.; Hideg, K.; Hubbell, W. L. *Biochemistry* **1996**, *35*, 7692−7704.
(14) Hubbell, W. L.; Cafisco, D. S.; Altenbach, C. *Nat. Struct. Biol.* **2000**, *7*, 735−739.
(15) Hubbell, W. L.; Gross, A.; Langen, R.; Lietzow, M. A. *Curr. Opin. Struct. Biol.* **1998**, *8*, 649−656.
(16) Colunbus, L.; Hubbell, W. L. *TIBS* **2002**, *27*, 288−295.
(17) Tombolato, F.; Ferrarini, A.; Freed, J. H. *J. Phys. Chem. B* **2006**, *110*, 26248−26259.
(18) Tombolato, F.; Ferrarini, A.; Freed, J. H. *J. Phys. Chem. B* **2006**, *110*, 26260−26271.
(19) Polimeno, A.; Freed, J. H. *Adv. Chem. Phys.* **1993**, *83*, 89−206.
(20) Polimeno, A.; Freed, J. H. *J. Phys. Chem.* **1995**, *99*, 10995−11006.
(21) Liang, Z.; Freed, J. H. *J. Phys. Chem. B* **1999**, *103*, 6384−6396.
(22) Barnes, J. P.; Liang, Z.; McHaourab, H. S.; Freed, J. H. *Biophys. J.* **1999**, *76*, 3298−3306.
(23) Liang, Z.; Lou, Y.; Freed, J. H.; Columbus, L.; Hubbell, W. L. *J. Phys. Chem. B* **2004**, *108*, 17649−17659.
(24) Zhang, Z.; Fleissner, M.; Tipikin, D.; Liang, Z.; Moscicki, J. K.; Earle, K. A.; Hubbell, W. J.; Freed, J. H. *J. Phys. Chem. B* **2010**, *114*, 5503−5521.
(25) Mittermaier, A.; Kay, J. E. *Science* **2006**, *312*, 224−228.
(26) Igumenova, T. I.; Frederick, K. K.; Wand, A. J. *Chem. Rev.* **2006**, *106*, 1672−1699.
(27) Jarymowycz, V. A.; Stone, M. J. *Chem. Rev.* **2006**, *106*, 1624−1671.
(28) Lipari, G.; Szabo, A. *J. Am. Chem. Soc.* **1982**, *104*, 4546−4559.
(29) Lipari, G.; Szabo, A. *J. Am. Chem. Soc.* **1982**, *104*, 4559−4570.
(30) Clore, G. M.; Szabo, A.; Bax, A.; Kay, L. E.; Driscoll, P. C.; Gronenborn, A. M. *J. Am. Chem. Soc.* **1990**, *112*, 4989−4991.
(31) Tugarinov, V.; Liang, Z.; Shapiro, Yu. E.; Freed, J. H.; Meirovitch, E. *J. Am. Chem. Soc.* **2001**, *123*, 3055−3063.
(32) Meirovitch, E.; Shapiro, Yu. E.; Polimeno, A.; Freed, J. H. *J. Phys. Chem. A* **2006**, *110*, 8366−8396.
(33) Meirovitch, E.; Shapiro, Yu. E.; Polimeno, A.; Freed, J. H. *Prog. NMR Spectrosc.* **2010**, *56*, 360−405.
(34) Zerbetto, M.; Polimeno, A.; Meirovitch, E. *J. Phys. Chem. B.* **2009**, *113*, 13613−13625.
(35) Tugarinov, V.; Shapiro, Yu. E.; Liang, Z.; Freed, J. H.; Meirovitch, E. *J. Mol. Biol.* **2002**, *315*, 155−170.
(36) Shapiro, Yu. E.; Kahana, E.; Tugarinov, V.; Liang, Z.; Freed, J. H.; Meirovitch, E. *Biochemistry* **2002**, *41*, 6271−6281.
(37) Shapiro, Yu. E.; Meirovitch, E. *J. Phys. Chem. B* **2006**, *110*, 11519−11524.
(38) Shapiro, Yu. E.; Kahana, E.; Meirovitch, E. *J. Phys. Chem. B* **2009**, *113*, 12050−12060.
(39) Shapiro, Yu. E.; Meirovitch, E.. *J. Phys. Chem. B* **2009**, *113*, 7003−7011.
(40) Meirovitch, E.; Zerbetto, M.; Polimeno, A.; Freed, J. H. *J. Phys. Chem.B* **2011**, *115*, 143−157.
(41) E. Meirovitch, E.; Polimeno, A.; Freed, J. H. Protein Dynamics by NMR Spin Relaxation: The Slowly Relaxing Local Structure Perspective In *Encyclopedia of Magnetic Resonance*; Harris, R. K., Wasylishen, R. E., Eds.; John Wiley: Chichester, U.K.; DOI: 10.1002/9780470034590.emrstm1243, 2011.
(42) Meirovitch, E.; Shapiro, Yu. E.; Zerbetto, M.; Polimeno, A. *J. Phys. Chem. B* **2012**, *116*, 886−894.
(43) Lienin, S. F.; Bremi, T.; Brutscher, B.; Brüschweiler, R.; Ernst, R. R. *J. Am. Chem. Soc.* **1998**, *120*, 9870−9879.
(44) Bernado, P.; Blackledge, M. *J. Am. Chem. Soc.* **2004**, *126*, 7760−7761.
(45) Bouvignies, G.; Bernado, P.; Meier, S.; Cho, K.; Grzesiek, S.; Brüschweiler, R.; Blackledge, M. *Proc. Natl. Acad. Sci. U.S.A.* **2005**, *102*, 13885−13890.
(46) Clore, G. M.; Schwieters, C. D. *Biochemistry* **2004**, *43*, 10678−10691.
(47) Buck., M.; Karplus, M. *J. Am. Chem. Soc.* **1999**, *121*, 9645−9658.
(48) Fadel, A. R.; Jin, D. Q.; Montelione, G. T.; Levy, R. M. *J. Biomol. NMR* **1995**, *6*, 221−226.
(49) *The Molecular Dynamics of Liquid Crystals*; Luckhurst, G. R., Veracini, C. A., Eds.; Kluwer Academic Publishers: The Netherlands, 1994; Chapter 12.
(50) Goldman, M. *J. Magn. Reson.* **1984**, *60*, 437−452.
(51) Tjandra, N.; Szabo, A.; Bax, A. *J. Am. Chem. Soc.* **1996**, *118*, 6986−6991.
(52) Kroenke, C. D.; Loria, J. P.; Lee, L. K.; Rance., M.; Palmer, A. G., III. *J. Am. Chem. Soc.* **1998**, *120*, 7905−7915.
(53) Abragam, A. *Principles of Nuclear Magnetism*; Oxford University Press (Clarendon): London, 1961.
(54) Peng, J. W.; Wagner, G.; James, T. L.; Oppenheimer, N. J. *Methods Enzymol.* **1994**, *239*, 563−595.
(55) Cavanagh, J.; Fairbrother, W. J.; Palmer, A. G., III; Skelton, N. J. *Protein NMR Spectroscopy: Principles and Applcation*; Academic Press, San Diego, CA, 1996.
(56) Brink, D. M.; Satchler, G. R. *Angular Momentum*; Clarendon Press: Oxford, U.K., 1968.
(57) Freed, J. H. *J. Chem. Phys.* **1977**, *66*, 4183−4199.
(58) Lin, W.-J.; Freed, J. H. *J. Phys. Chem.* **1979**, *83*, 379−401.
(59) Halle, B. *J. Chem. Phys.* **2009**, *131*, 224507−22.
(60) Farrow, N. A.; Muhandiram, R.; Singer, A.; Pascal, S. M.; Kay, C. M.; Gish, G.; Shoelson, S. E.; Pawson, J.; Forman-Kay, J. D.; Kay, L. E. *Biochemistry* **1994**, *33*, 5984−6003.
(61) Lee, L. K.; Rance, M.; Chazin, W. J.; Palmer, A. G. H., III *J. Biomol. NMR* **1997**, *9*, 287−298.
(62) Brüschweiler, R.; Liao, X.; Wright, P. E. *Science* **1995**, *268*, 886−889.
(63) Pang, Y.; Buck, M.; Zuiderweg, E. R. P. *Biochemistry* **2002**, *41*, 2655−2666.
(64) Fushman, D.; Cahill, S.; Cowburn, D. *J. Mol. Biol.* **1997**, *266*, 173−194.
(65) Case, D. *Acc. Chem. Res.* **2002**, *35*, 325−331.
(66) Srynnikov, N. R.; Millet, O.; Kay, L. E. *J. Am. Chem. Soc.* **2002**, *124*, 6449−6460.
(67) Meirovitch, E.; Shapiro, Yu. E.; Zerbetto, M.; Polimeno, A. *J. Phys. Chem. B* **2012**, *116*, 886−894.
(68) Shapiro, Yu. E.; Meirovitch, E. *J. Phys. Chem. B.* **2012**, *116*, 4056−4068.
(69) Mathews, C. K.; van Holde, K. E.; Ahern, K. G. *Biochemistry*, 3rd ed.; Addison Wesley Longman, Inc.: Reading, MA, U.S.A., 1999.